REGULAR ARTICLE

Decoherence mitigation by embedding a logical qubit in a qudit

Hideyuki Miyahara[1] · Yiyou Chen[2] · Vwani Roychowdhury[1,3] ·
Louis-Serge Bouchard[3,4,5]

Abstract

Quantum information stored in a qubit is rapidly lost to the environment. The realization of robust qubits is one of the most important challenges in quantum computing. Herein, we propose to embed a logical qubit within the manifold of a qudit as a scheme to preserve quantum information over extended periods of time. Under identical conditions (e.g., decoherence channels), the submanifold of the logical qubit exhibits extended lifetimes compared to a pure two-level system (qubit). The retention of quantum information further improves with separation between the sublevels of the logical qubit. Lifetime enhancement can be understood in terms of entropy production of the encoding and nonencoding subspaces during evolution under a quantum map for a d-level system. The additional pathways for coherent evolution through intermediate sublevels within a d-level manifold provide an information-preserving mechanism: reversible alternative channels to the irreversible loss of information to the environment characteristic of open quantum systems.

✉ Louis-Serge Bouchard
   louis.bouchard@gmail.com

   Hideyuki Miyahara
   miyahara@ist.hokudai.ac.jp; hmiyahara512@gmail.com

   Yiyou Chen
   gerry99@ucla.edu

   Vwani Roychowdhury
   vwani@g.ucla.edu

[1] Department of Electrical and Computer Engineering, University of California, Los Angeles, CA 90095, USA

[2] Department of Computer Science, University of California, Los Angeles, CA 90095, USA

[3] Center for Quantum Science and Engineering, University of California, Los Angeles, CA 90095, USA

[4] Department of Chemistry and Biochemistry, University of California, Los Angeles, CA 90095, USA

[5] California NanoSystems Institute, University of California, Los Angeles, CA 90095, USA

 ⧄ Springer

1 Introduction

Schemes for quantum computation (QC) rely on networks of quantum bits (qubits) that are mutually coupled and subjected to sequences of controlled operations (quantum gates). Each individual qubit is represented by an algebra of zero-trace 2×2 unitary Hermitian matrices, while a classical computer utilizes classical bits that take the value 0 or 1 [1–4]. The resulting topological manifold describing the state of the qubit is the Bloch sphere, which encodes an uncountably infinite number of possible states, as compared to the two discrete states of a classical bit. Because Hilbert spaces are complex projective spaces, the points on the Bloch sphere are isomorphic to the unit vectors in $\mathbb{C}^2$, representing the probabilistic outcomes of observing $| 0 \rangle$ and $| 1 \rangle$ under projective measurements. Multi-qubit states are linear combinations of vectors that are constructed from tensor products of single-qubit computational basis vectors, i.e., $| \psi \rangle = \sum_{\vec{q}} a_{\vec{q}} \mid \alpha_{q_1} \rangle \otimes \mid \alpha_{q_2} \rangle \otimes \cdots \otimes \mid \alpha_{q_n} \rangle$. The richness of information encoded by qubits endow quantum computers with unique computational capabilities. Early on, Shor [5, 6] Grover [7] proposed algorithms that have almost become synonymous with QC. Unfortunately, the creation of clean quantum gates exhibiting high fidelity in the presence of decoherence have proven to be a formidable challenge. Quantum error correction (QEC) codes were proposed to mitigate these problems [8, 9]. The highly important toric and surface codes have had a great impact in the field [9–16]. Improvements in quantum technology over the last two decades have led to the successful realization of the surface code [17, 18]; see also [19, 20].

There currently exist several different schemes for the realization of physical qubits (e.g., molecular magnets [21], defects in solids, cold ions, atoms and molecules, Rydberg atoms, nuclear and electron spin resonances, to name a few); superconducting qubit platforms are currently the most popular thanks to their public availability on cloud computing platforms made possible by companies such as Google, IBM, Rigetti, and IonQ [22]. These platforms are termed NISQ (noisy intermediate scale quantum) devices. As pointed out by Preskill [23], NISQ devices have found many immediate applications, such as variational quantum algorithms [24–27] and quantum-inspired algorithms [28–31]. As of today, it is unclear whether any of these methods provide a clear quantum advantage over classical computers in applications of current interest. We note, on the other hand, that the feasibility of quantum supremacy has been demonstrated in experiments [18].

Indeed, while these NISQ platforms provide excellent research, development and educational tools, the realization of large-scale QC algorithms remains out of reach, as the qubits remain too fragile, not well-controlled, and limited by decoherence as well as leakage effects. The impact of quantum errors can be mitigated using error correction schemes. However, those are based on fault-tolerant architectures, which require additional hardware resources (qubits and related controls). The added overhead limits the usefulness of error correction schemes. To overcome this problem, physical devices that are inherently fault tolerant have been proposed as a way to overcome logical errors [32]. With physical fault tolerance, no special architectures are needed,

as the fault tolerance is built into the design of the qubit itself. This circumvents the problem of different setups producing different sources of errors. In this context, the realization of robust qubits is of great interest and utmost importance.

In the context of generating robust qubits, we note the proposals for multi-level systems, such as error-correcting codes for molecular magnets [33, 34], optical systems [35] as well as the Kerr-cat qubit (superposition of coherent states) [36]. In Ref. [37], the authors proposed molecular spin qudits as elements of a quantum simulator. In Ref. [38], dysprosium (Dy), whose spin J is 8, was used for enhanced quantum sensing. Furthermore, bosonic codes have been extensively studied: the binomial code [39], the cat code [40–44], the Gottesman–Kitaev–Preskill (GKP) code [36, 45–48], and the rotation-symmetric bosonic codes [49]. To realize the bosonic codes, truncated bosonic modes are required and optical systems are possible platforms that may provide us with bosonic modes. Nuclear spins with $I > 1/2$ are examples of multi-level spin systems, and they exhibit faster relaxation rates, which are a function of the nuclear quadrupole moment and local electric-field gradient. In Ref. [50–53], the structure and control of such systems are analyzed in the context of NMR experiments.

The description of qudit systems and their uses in QC is often done in terms of generalized Pauli and Clifford operators [54], qudit stabilizer code [55, 56], qudit surface code [57], a decoder for the qudit surface code [58], and a quantum error correction architecture for qudits [59, 60]. Finally, in Ref. [61] qudit-based QC is discussed, including implementations of qudit variants of known quantum algorithms. In this study, we examine the case of qudits (d-level systems) that encode quantum states in a superposition of two energy sublevels playing the role(s) of logical qubits. The remaining unused levels (the "nonencoding subspace") are not explicitly addressed. Instead, this subspace naturally enhances the lifetime of the logical qubits. We focus on the spin–lattice relaxation mechanism, where enhanced relaxation motivates the use of such systems in quantum memory applications. Specifically, we show that when the quantum information is stored into the two most polarized spin states (e.g., $| \psi \rangle = c_1 | d - 1 \rangle + c_2 | 0 \rangle$), one obtains a more robust quantum memory in which quantum information can be stored for longer periods of time compared to a pure two-level system (qubit) with no intermediate sublevels separating the pair of qubit levels. In numerical computations, we show that the lifetime of the proposed quantum memory is longer than the conventional qubit system. In order to understand the flow of information between encoding and nonencoding subspaces, entropy production provides an explanation for why qudits exhibit fundamentally different behavior compared to qubits. This paper is organized as follows. In Sects. 2, 4, and 5, we describe the mathematical prerequisite. In Sects. 6 and 7, we show numerical simulations and give discussions. Finally, Sect. 8 concludes this paper. In "Appendix," we compare the qudit embedding method to a simple QEC model and identify a potentially interesting direction for future research, namely, the use of qudits in quantum memory applications with inherent robustness to information loss.

2 Maximally polarized states (spin-coherent states) in qudits

In this section, we describe how to embed qubit information into a qudit system. Consider a qudit with spin s whose Hilbert space is spanned by $d = 2s + 1$ energy levels. The density matrix for a qubit $\hat{\rho}'$ is specified via two basis states $|\uparrow\rangle, |\downarrow\rangle$ and four complex numbers $\rho_{\uparrow\uparrow}, \rho_{\uparrow\downarrow}, \rho_{\downarrow\uparrow}, \rho_{\downarrow\downarrow}$ that satisfy $\rho_{\uparrow\uparrow} + \rho_{\downarrow\downarrow} = 1$ and $\rho_{\uparrow\downarrow}^* = \rho_{\downarrow\uparrow}$:

$$\hat{\rho}' := \rho_{\uparrow\uparrow} |\uparrow\rangle\langle\uparrow| + \rho_{\uparrow\downarrow} |\uparrow\rangle\langle\downarrow| + \rho_{\downarrow\uparrow} |\downarrow\rangle\langle\uparrow| + \rho_{\downarrow\downarrow} |\downarrow\rangle\langle\downarrow|. \tag{1}$$

We denote a single-*qudit* state by $\hat{\rho}$ and the d states in the d-level qudit by $|0\rangle, |1\rangle, |2\rangle, \ldots, |d-1\rangle$. The state described in Eq. (1) is encoded into the d-level qudit as follows:

$$\begin{aligned}\hat{\rho} := {} & \rho_{\uparrow\uparrow} |0\rangle\langle 0| + \rho_{\uparrow\downarrow} |0\rangle\langle d-1| \\ & + \rho_{\downarrow\uparrow} |d-1\rangle\langle 0| + \rho_{\downarrow\downarrow} |d-1\rangle\langle d-1|.\end{aligned} \tag{2}$$

Note that $|0\rangle$ and $|d-1\rangle$ are often referred to as $|s, s\rangle$ and $|s, -s\rangle$, respectively. They are also called "maximally polarized" states. In this paper, we investigate some properties of Eq. (2), such as its lifetime by using an error model that will be explained below. Our analysis shows that encoding of the qubit state in the maximally polarized states leads to longer lifetimes compared to the use of intermediate levels.

3 Error models

We start by defining the generalized Pauli operators [62]:

$$\hat{X}' := \sum_{k=0,1,\ldots,d-2} (|k\rangle\langle k+1| + |k+1\rangle\langle k|). \tag{3}$$

$$\hat{Z} := \sum_{k=0,1,\ldots,d-1} \omega^k |k\rangle\langle k|, \tag{4}$$

where $\omega := e^{2\pi i/d}$. Note that the definition of $\hat{X}'$ in Eq. (3) is different from the definition of $\hat{X}$ in Ref. [62] since $\hat{X}$ is not symmetric. As justified in A.4 of "Appendix," there exist physical models where symmetric X-errors occur. We therefore use $\hat{X}'$ to represent that class of error. For a n-qudit system, $\hat{X}'$ in Eq. (3) and $\hat{Z}$ in Eq. (4) acting on the ith qudit are denoted by

$$\hat{X}'_i := \underbrace{\hat{1} \otimes \cdots \otimes \hat{1}}_{i-1} \otimes \hat{X}' \otimes \underbrace{\hat{1} \otimes \cdots \otimes \hat{1}}_{n-i}, \tag{5}$$

$$\hat{Z}_i := \underbrace{\hat{1} \otimes \cdots \otimes \hat{1}}_{i-1} \otimes \hat{Z} \otimes \underbrace{\hat{1} \otimes \cdots \otimes \hat{1}}_{n-i}. \tag{6}$$

Evolution of open quantum systems is continuous in time, as described by a master equation such as the Lindblad equation [63]. However, in the QEC literature it is

customary to consider a discrete-time dynamical model called the quantum map:

$$\hat{\rho}_{t+\Delta t} = \mathcal{E}_p(\hat{\rho}_t), \tag{7}$$

where Δt is a discrete-time step taken to be $\Delta t = 1$ (without loss of generality). For $\mathcal{E}_p(\cdot)$ in Eq. (10), we consider the following model:

$$\mathcal{E}_p(\cdot) := \bigodot_{i=1,2,...,n} \mathcal{E}_p(\cdot; \{\hat{K}_{i,k}\}_{k=1}^{d-1}), \tag{8}$$

where

$$\begin{aligned}
\bigodot_{i=1,2,...,n} & \mathcal{E}_p(\cdot; \{\hat{K}_{i,k}\}_{k=1}^{K}) \\
& := \mathcal{E}_p(\mathcal{E}_p(\ldots (\mathcal{E}_p(\cdot; \{\hat{K}_{n,k}\}_{k=1}^{K}) \ldots; \{\hat{K}_{2,k}\}_{k=1}^{K}); \{\hat{K}_{1,k}\}_{k=1}^{K}),
\end{aligned} \tag{9}$$

and

$$\mathcal{E}_p(\hat{\rho}; \{\hat{K}_{i,k}\}_{k=1}^{K}) := (1-p)\hat{\rho} + \frac{p}{K} \sum_{k=1}^{K} \frac{\hat{K}_{i,k}\hat{\rho}\hat{K}_{i,k}^{\dagger}}{\mathrm{Tr}[\hat{K}_{i,k}\hat{\rho}\hat{K}_{i,k}^{\dagger}]}. \tag{10}$$

Note that the notation used in Eq. (8) is not the tensor product. It merely denotes the composition of operations, as shown in Eq. (9). Here, p is the probability of error in the model and K is the number of error channels. For the X'-type error model and the Z-type error model, $K = 1$, but for the $X' + Z$-type error model, $K = 2$. For $\mathcal{E}_p(\hat{\rho}; \{\hat{K}_{i,k}\}_{k=1}^{K})$ in Eq. (10) being trace-preserving, we have divided the second term of the right-hand side of Eq. (10) by $\mathrm{Tr}[\hat{K}_{i,k}\hat{\rho}\hat{K}_{i,k}^{\dagger}]$. Note that in general, $\mathrm{Tr}[\hat{K}_{i,k}\hat{\rho}\hat{K}_{i,k}^{\dagger}]$ can be zero, but we have checked that in our setup, it is nonzero. Single-qudit operators, $\{\hat{K}_{i,k}\}_{\substack{k=1,2,...,K, \\ i=1,2,...,n}}$, are denoted as:

$$\hat{K}_{i,k} := \underbrace{\hat{1} \otimes \cdots \otimes \hat{1}}_{i-1} \otimes \hat{K}_k \otimes \underbrace{\hat{1} \otimes \cdots \otimes \hat{1}}_{n-i}. \tag{11}$$

Note that $\bigodot_{i=1,2,...,n} \mathcal{E}_p(\cdot; \{\hat{K}_{i,k}\}_{k=1}^{K})$ does not depend on the order of terms in the product since we consider only single-qudit errors.

4 Process fidelity

A variety of measures [64] exist to quantify the time evolution of quantum states. We use the process fidelity [65, 66] since our calculations do not invoke a random number generator (e.g., the Haar measure) and its interpretation is relatively clear. The definition of process fidelity is based on the concept of quantum state fidelity for the maximally entangled state. Maximally entangled state is used because the

dynamics of decoherence depends on not only maps but also initial states. When we consider the maximally entangled state and an error model (map) is applied to only one of them, fidelity appears to be monotonically decreasing. The fidelity between two quantum states $\hat{\rho}$ and $\hat{\sigma}$ is given by [64]

$$\mathcal{F}(\hat{\rho}, \hat{\sigma}) := \left(\mathrm{Tr} \left[\sqrt{\sqrt{\hat{\rho}} \hat{\sigma} \sqrt{\hat{\rho}}} \right] \right)^2 . \tag{12}$$

The initial state is

$$| \psi_{\mathrm{ini}} \rangle = \frac{1}{\sqrt{2}} (| 0_{\mathrm{L}} \rangle \otimes | 0_{\mathrm{L}} \rangle + | 1_{\mathrm{L}} \rangle \otimes | 1_{\mathrm{L}} \rangle), \tag{13}$$

whereas error models are applied to the second qudit. We compute the fidelity between the initial state and the state at time step τ.

The general definition of the process fidelity is given by [65, 66]

$$\mathcal{F}(\mathcal{A}(\cdot), \mathcal{B}(\cdot)) := \mathcal{F}(\hat{\rho}_{\mathcal{A}}, \hat{\rho}'_{\mathcal{B}}), \tag{14}$$

where $\hat{\rho}_{\mathcal{A}} := \mathcal{A}(\hat{\rho})$ and $\hat{\rho}'_{\mathcal{B}} := \mathcal{B}(\hat{\rho}')$. In this study, we use the identity map for $\mathcal{A}$ in Eq. (14) and the error maps defined in Sect. 3.

5 Entropy production

To interpret the results from numerical simulations, we used entropy production, which is defined as

$$\Delta S_{\tau} := S_{\tau} - S_{\tau - 1}, \tag{15}$$

with $S_{-1} = 0$ and $S := -\mathrm{Tr}[\hat{\rho} \ln \hat{\rho}]$. Furthermore, we define entropy productions in the total space, the encoding subspace, and the nonencoding subspace in terms Eq. (15) with $\hat{\rho}$, $\hat{\rho}^{\mathrm{en}}$, and $\hat{\rho}^{\mathrm{non-en}}$, respectively, where
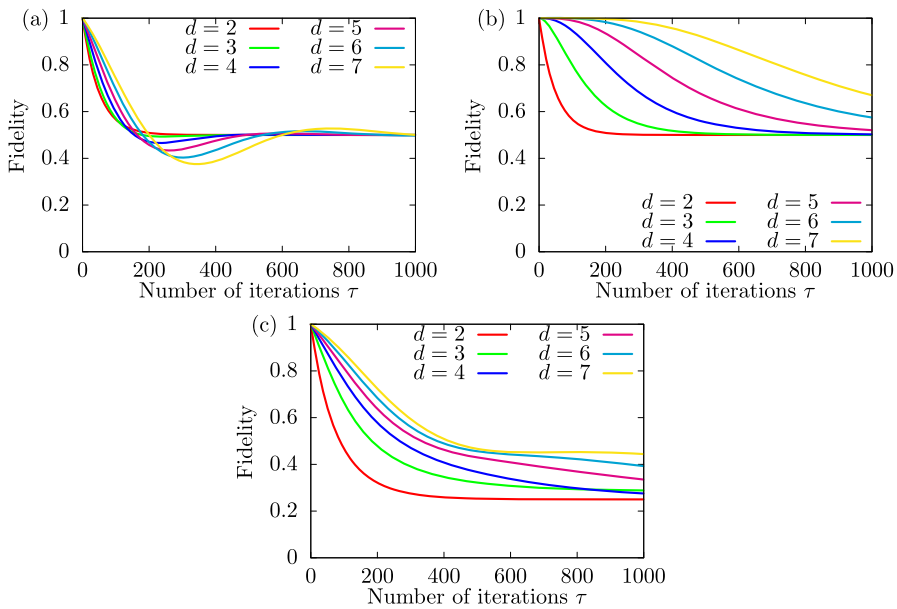
$$\hat{\rho}^{\mathrm{en}} := \hat{P}^{\mathrm{en}} \hat{\rho} \hat{P}^{\mathrm{en}}, \tag{16}$$

$$\hat{\rho}^{\mathrm{non-en}} := \hat{Q}^{\mathrm{en}} \hat{\rho} \hat{Q}^{\mathrm{en}}. \tag{17}$$

Here, $\hat{P}^{\mathrm{en}}$ is the projection onto the most polarized states $| 0_{\mathrm{L}} \rangle$ and $| 1_{\mathrm{L}} \rangle$, whereas $\hat{Q}^{\mathrm{en}}$ is the projection in the orthogonal complement of $\hat{P}^{\mathrm{en}}$ (i.e., the nonencoding subspace):

$$\hat{P}^{\mathrm{en}} := (| 0_{\mathrm{L}} \rangle \langle 0_{\mathrm{L}} | + | 1_{\mathrm{L}} \rangle \langle 1_{\mathrm{L}} |) \otimes (| 0_{\mathrm{L}} \rangle \langle 0_{\mathrm{L}} | + | 1_{\mathrm{L}} \rangle \langle 1_{\mathrm{L}} |), \tag{18}$$

$$\hat{Q}^{\mathrm{en}} := \hat{1} - \hat{P}^{\mathrm{en}}. \tag{19}$$

Fig. 1 Process fidelity for **a** the Z-type error model, **b** the X'-type error model, and **c** the $X' + Z$-type error model. d is varied. The initial state is the maximally entangled state. The process fidelity decays slower for higher d, and this observation means that qudits with higher d show longer life times. The maximally polarized state is used: $|0_L\rangle = |0\rangle$ and $|1_L\rangle = |d-1\rangle$ where d is the number of energy levels

6 Numerical simulation: fidelity

To quantify decoherence of quantum states, we use the process fidelity, Eq. (12), by computing the quantity:

$$\mathcal{F}\left(\hat{\rho}_{\mathrm{ini}}, \frac{\hat{\rho}_t^{\mathrm{en}}}{\mathrm{Tr}[\hat{\rho}_t^{\mathrm{en}}]}\right), \tag{20}$$

where $\hat{\rho}_t^{\mathrm{en}} := \hat{P}^{\mathrm{en}} \hat{\rho}_t \hat{P}^{\mathrm{en}}$ and $\hat{\rho}_t$ is defined, recursively, via $\hat{\rho}_t = \mathcal{E}_p(\hat{\rho}_{t-1})$. We denote the actions of the qudit operators $\hat{X}'_i$, $\hat{Z}_i$ and $\hat{X}'_i + \hat{Z}_i$ in Eq. (8) by $\mathcal{E}_p^{(X')}(\cdot)$, $\mathcal{E}_p^{(Z)}(\cdot)$, and $\mathcal{E}_p^{(X'+Z)}(\cdot)$, respectively. Figure 1 shows process fidelity for the Z-, X'-, and $X'+Z$-type error models and its dependence on d. Here, we take $|0_L\rangle = |0\rangle$ and $|1_L\rangle = |d-1\rangle$ (maximally polarized state) and increase the dimensionality of the qudit manifold (d).

For all three error models, process fidelity increases with d, at least initially. Thus, quantum information is preserved over longer times. The logical qubit's lifetime appears to increase with its dimensionality (d). It is still unclear whether this is due to dimensionality or separation between the levels of the logical qudit. We observe non-monotonic behavior in Fig. 1a. The fidelity initially drops because the errors move the "weights" away from the most polarized levels to intermediate levels. After several steps, all levels possess nonzero "weights," and some weights begin to flow back to the most polarized levels at a higher rate, resulting in higher fidelity. Mathematically, the
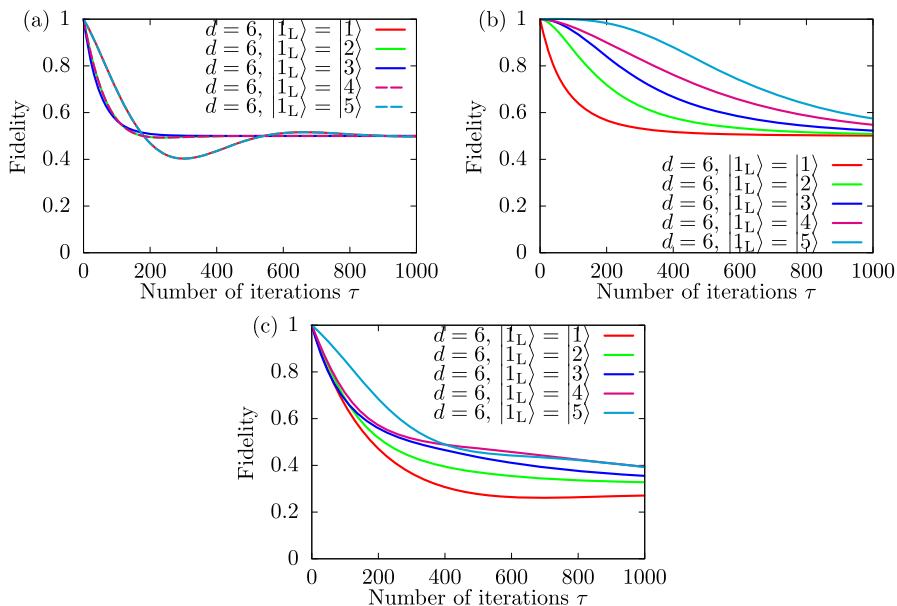
Fig. 2 Process fidelity for **a** the Z-type error model, **b** the X'-type error model, and **c** the $X' + Z$-type error model. We have varied $|1_L\rangle$ from $|1\rangle$ to $|5\rangle$, while $|0_L\rangle$ is fixed to $|0\rangle$. The initial state is the maximally entangled state
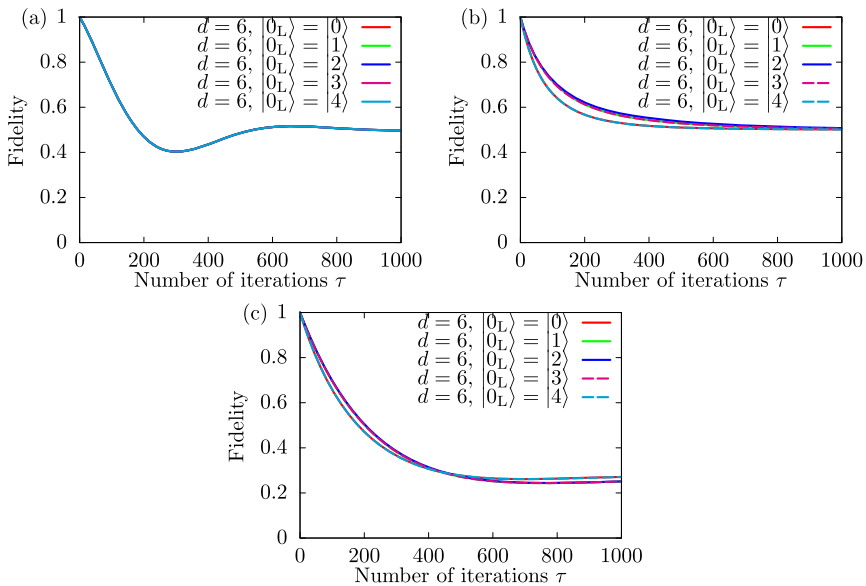
Fig. 3 Process fidelity for the X'-type error model. We have varied the number of levels from $d = 2$ to $d = 6$. We have varied $|1_L\rangle$ from $|1\rangle$ to $|5\rangle$, while $|0_L\rangle$ is fixed to $|0\rangle$
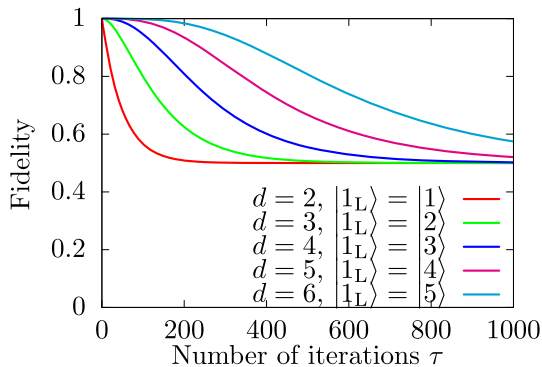
time evolution of the population of any given sublevel is dictated by a set of coupled ODEs (one for each sublevel and coupling to its neighboring levels), and such coupled ODEs generally lead to non-exponential decays.

To investigate this, we fix the value $d = 6$ as well as the state $|0_L\rangle = |0\rangle$ but vary the distance between two logical states by increasing $|1_L\rangle$. In Fig. 2, we show the $|1_L\rangle$-dependence of the process fidelity for the Z-, X'- and $X' + Z$-type error models.

The observed trends are similar to those of Fig. 1. We therefore conclude that the distance between $|0_L\rangle$ and $|1_L\rangle$ is the key factor, not the dimensionality of the qudit itself (although dimensionality d needs to be high). Figure 3 shows that the lifetime

Fig. 4 Process fidelity for **a** the Z-type error model, **b** the X'-type error model, and **c** the $X' + Z$-type error model. We have varied $| 0_L \rangle$ and $| 1_L \rangle$ simultaneously keeping the distance: $| 1_L \rangle = | n + 1 \rangle$ when $| 0_L \rangle = | n \rangle$. The initial state is the maximally entangled state

enhancement holds regardless of whether d is fixed and the logical qubit $| 1_L \rangle$ is increased, or if d is varied along with $| 1_L \rangle$.

In Fig. 4, we show process fidelity when we vary $| 0_L \rangle$ and $| 1_L \rangle$ simultaneously while keeping the distance fixed (set equal to 1).

All curves are nearly identical, meaning that the lifetime does not depend on the choice of sublevels. This result supports the view that lifetime depends primarily on distance between levels.

Thus, the process fidelity decays slower as the separation between logical levels is increased. Consider the experiment where d is increased and the logical qubit is encoded in the maximally polarized states. We fit the Kohlrausch (stretched exponential) function [67, 68]

$$f(t; b, \tau, \alpha) := (1 - b)e^{-(t/\tau)^{\alpha}} + b. \tag{21}$$

for each d and obtain its parameters α, τ, and b. (A parameter estimation method was proposed in Ref. [69].) In Table 1, the values of b, τ, and α obtained from the fit are shown.

In Fig. 5a, the results shown in Table 1 are plotted and, in Fig. 5b, the raw values and the fitting curves are shown.

Figure 5b shows good agreement between raw data (symbols) and the fitted curve. The value of α increases from 1 to ~ 2, whereas the lifetime τ increases by a factor of ~ 15 (more than an order of magnitude). This result for τ is important, as it supports the use of qudits as building blocks for more robust quantum memories. The result

Table 1 Estimated values of b, τ, and α for each d

| d	b	τ	α
2	0.500	49.498	1.000
3	0.500	161.053	1.417
4	0.500	307.247	1.720
5	0.500	490.644	1.921
6	0.501	718.775	2.060
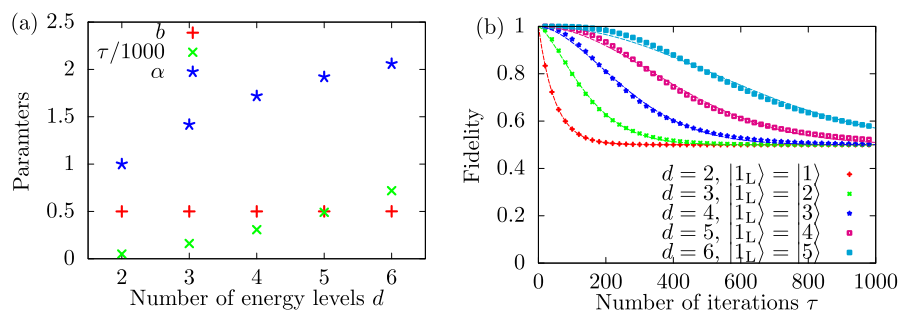
Fig. 5 Estimated parameters of the fitted Kohlrausch function for the process fidelity in the case of the X'-type error model. **a** Dependence of b, τ, and α on d. **b** Raw data and fitting curves. The original data are shown in dots and the fitting curves are depicted via dashed lines. We have varied $|1_{\mathrm{L}}\rangle$ from $|1\rangle$ to $|5\rangle$, while $|0_{\mathrm{L}}\rangle$ is fixed to $|0\rangle$

for α indicates that for the X' error model. This can be understood from the form of the X' operator (Eq. 3) which, when inserted into the quantum map (Eq. 10), leads to a set of coupled ODEs for the elements of the density matrix that describe a detailed balanced first-order rate process with transitions between neighboring levels. It is well known that distributions of rate processes lead to stretched exponential relaxation.

7 Numerical simulation: entropy production

To shed light on the results of Sect. 6, we compute entropy production (defined in Sect. 5). Figure 6 shows entropy production of the total space, the encoding subspace, and the nonencoding subspace for the Z-type error model.

We see that in Fig. 6a entropy production decreases with d. This behavior is consistent with the results of Fig. 1a: Shorter lifetimes are associated with high entropy production (rapid loss of information). The results of Fig. 6 also show that entropy production in the encoding subspace and the total space are the same, but entropy production in the nonencoding subspace is always zero. We interpret this to mean that information initially stored in the logical qubit flows out of the qudit system. This leakage of information out of the system is less pronounced at large d. The lack of entropy production in the nonencoding subspace (Fig. 6b) is a consequence of the Z-type error model, which does not have any channels connecting encoding and nonencoding
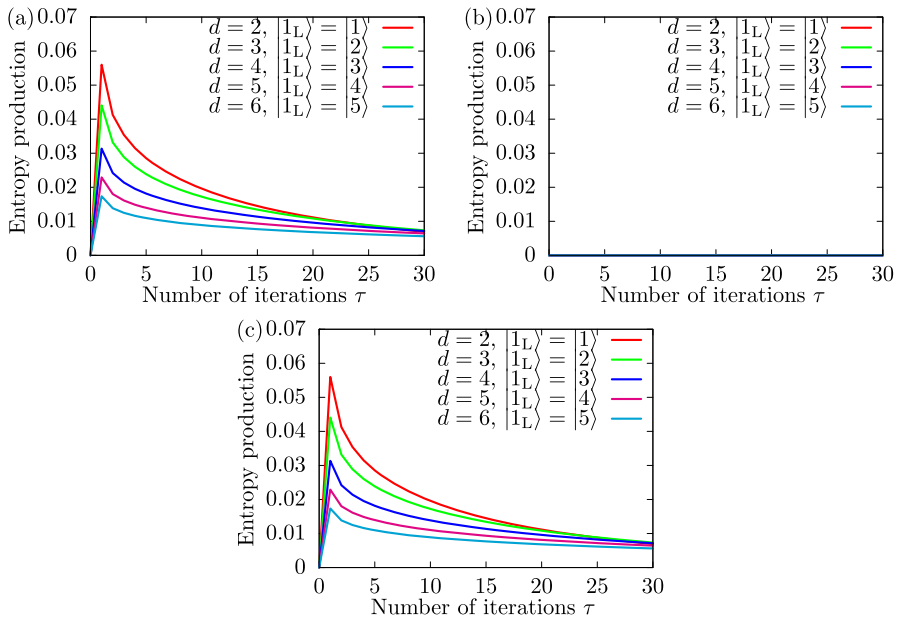
Fig. 6 Entropy production of **a** the encoding subspace, **b** the nonencoding subspace, and **c** the total space for the Z-type error model. The initial state is the maximally entangled state. The maximally polarized state is used: $| 0_L \rangle = | 0 \rangle$ and $| 1_L \rangle = | d - 1 \rangle$, where d is the number of energy levels

subspaces (i.e., none of the operators $| k \rangle\langle k |$ present in Z connect pairs of energy levels).

Figure 7 shows entropy production of the total space, the encoding subspace, and the nonencoding for the X'-type error model.

In Fig. 7a, entropy production within the encoding subspace is drastically suppressed with d. This observation is again consistent with the results of Fig. 1(b) (i.e., longer lifetimes with increased d due to the preservation of information). However, there is an important difference between the cases of the X'-type error model and the Z-type error model. For X', the entropy production in the nonencoding subspace is nonzero. In fact, entropy production in the nonencoding subspace dominates. This feature enables recovery of qubit information by post-selection. Contrary to the case of the Z-type error model, the entropy production in the nonencoding subspace and the total space are nearly identical except for the case $d = 2$. This leads to increased robustness of the state in the encoding subspace. We note that for $d = 2$ the nonencoding subspace does not exist; therefore, $d = 2$ is an important exception. It is the reason why physical qubits are less ideally suited for use as quantum memories: The only allowed pathway for information transfer is irreversible, whereas for the qudit some of the leakage channels are reversible.

In Fig. 8, we show entropy production of the total space, the encoding subspace, and the nonencoding for the X'-type error model and Z-type error model.

In the case of the $X' + Z$-type error model, intermediate behavior between the above two cases is observed. Though the improvements become smaller compared to
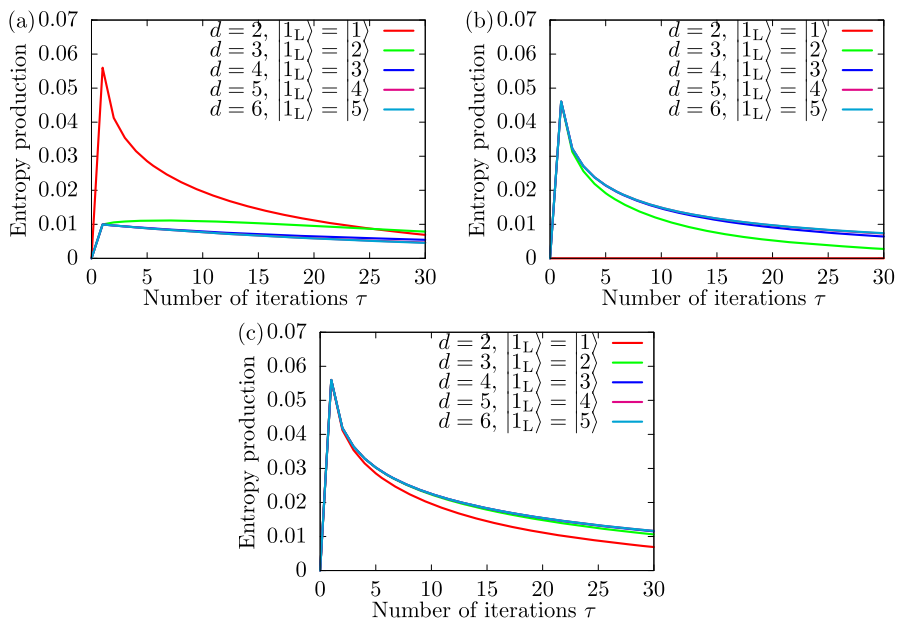
Fig. 7 Entropy production of **a** the encoding subspace, **b** the nonencoding subspace, and **c** the total space for the X'-type error model. The initial state is the maximally entangled state. The maximally polarized state is used: $|\,0_L\rangle =|\,0\rangle$ and $|\,1_L\rangle =|\,d-1\rangle$ where d is the number of energy levels
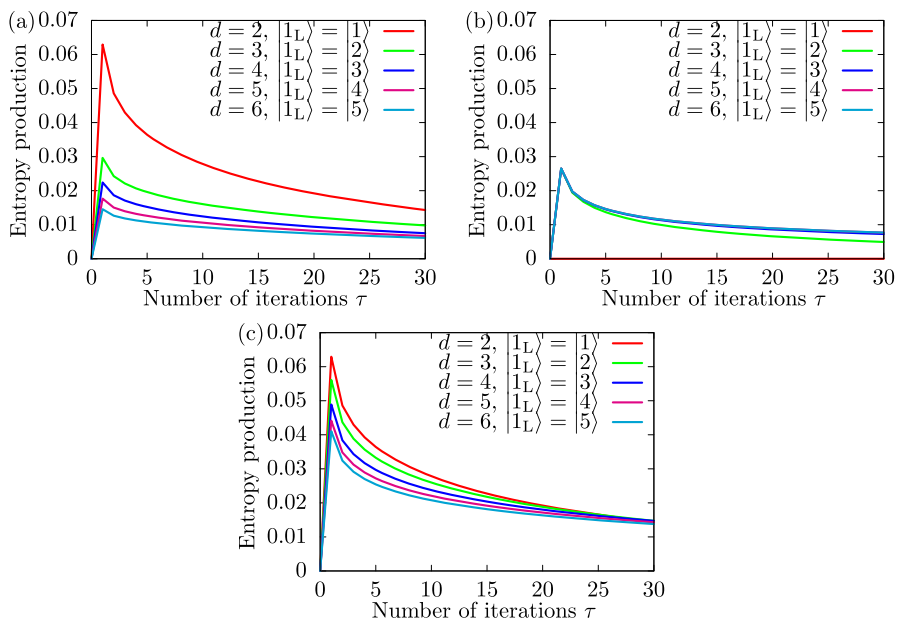
Fig. 8 Entropy production of **a** the encoding subspace, **b** the nonencoding subspace, and **c** the total space for the X'-type error model and Z-type error model. The initial state is the maximally entangled state. The maximally polarized state is used: $|\,0_L\rangle =|\,0\rangle$ and $|\,1_L\rangle =|\,d-1\rangle$, where d is the number of energy levels

the case of the pure X'-type error model, entropy production can still be suppressed by increasing d.

8 Conclusions

We propose the use of qudits as embedding space to encode quantum information from qubits. When the rates of all error channels are kept identical, the resulting quantum memory of the d-level system exhibits longer lifetime than the case of physical qubits. An interpretation of the results was obtained by computing entropy production within the encoding subspace: For the physical qubit, information loss is entirely irreversible, whereas for the qudit, information loss from the logical qubit state is only partly irreversible. The reversible part results in longer lifetimes. We show in "Appendix" that qudit encoding has properties analogous to quantum error correction (QEC).

These results suggest that the encoding of logical qubits in the levels of qudits can provide increased robustness due to the inherent physics of such systems. Interesting avenues to pursue would be to (i) explore how such physics-aided robustness—potentially requiring less extra overheads—compare with the algorithm-aided robustness created in QEC schemes, more specifically, estimating the circuit complexity of a QEC circuit that could afford similar robustness, and (ii) how to integrate the two schemes to obtain simpler circuits and reduced operation overheads that plague direct QEC implementations. In order to determine the actual performance gains, a real physical system and its precise characteristics should be modeled. Performance gains over QEC (if any) can only be determined by simulating the precise physical system under consideration, using realistic modeling. A proper QEC scheme for qudits must also be devised. "Appendix" presents a simple, but unoptimized one. Nonetheless, we conclude that these findings are encouraging and warrant further investigations. This work may lead to new strategies for quantum processors and quantum memories based on the use of qudits.

There are, of course, important physical considerations involved when using physical qudits, such as the faster relaxation rates of nuclei with large quadrupolar moments or the difficulty of selectively addressing pairs of sublevels. Optical qubits [70–72] and superconducting qubits could be adapted for such applications. Another possible test platform would be the nuclear spins in bullvalene in a liquid crystal solvent [73, 74]. Because of rapid bond shifting, every one of the ten protons is equivalent, and every dipolar coupling is the same; so the totally symmetric representation in such a system is effectively a spin-N system [74]. A simple $(X/2)$-τ-$(X/2)$ sequence will produce the theoretical maximum possible N-quantum coherence just by making the delay equal to $1/3D$ [74].

Data Availability Data sharing is not applicable to this article as no datasets were generated or analyzed during the current study.

Declarations

Conflict of interest We declare no conflicts of interest.

Appendix A: Limitations of QEC

Herein, we discuss some limitations of QEC and argue in favor of embedding quantum states inside maximally polarized qudit sublevels as a way to mitigate errors. The precise benefits of QEC (if any) of course may depend on the exact nature of the error model used, the precise physical nature of the qudits, and available control methods. The QEC model discussed here is limited to known physically plausible decoherence processes arising in multi-level systems (see section A.4). Better performing QEC is of course possible in theory (e.g., using an extended operator algebra such as one spanned by the set of monomials $X^n Z^m$), but may lack physical justification; such schemes are not discussed here.

A.1 Fate of maximally entangled states with QEC

Consider an isolated qudit with embedded logical qubit state (i.e., a quantum memory). The question we are interested in addressing is whether or not a stored quantum state can survive longer with or without QEC. Let us consider a simple QEC structure and investigate its properties.

A.1.1 Encoding scheme

In Ref. [59], a systematic approach to construct a circuit that embeds the measurement values of given stabilizer operators into ancilla qudits for the repetition code was proposed. We review the method.

Suppose that the initial state is $| \psi \rangle$. Consider the case where we want to embed n_s stabilizer operators $\{\hat{S}_i\}_{i=1}^{n_\text{s}}$ into a circuit. The redundant state, on which the repetition code relies, is given by

$$| \tilde{\psi} \rangle := \prod_{i=2,3,...,n_\text{r}} \widehat{\text{CNOT}}_{i,j} | \psi \rangle | \underbrace{00...0}_{n_\text{r}-1} \rangle, \tag{A1}$$

where n_r is the number of redundant qudits. Here, $\widehat{\text{CNOT}}_{i,j}$ is the CNOT gate whose control qudit is the ith qudit and target qudit is the jth qudit. Next, we define the

Fig. 9 QEC circuit for qudit syndrome measurements. $\hat{E}$ is an error operator
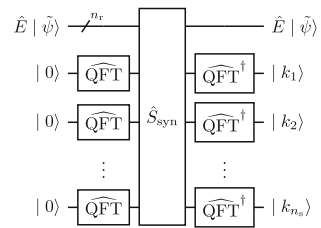
syndrome detection operator $\hat{S}_{\mathrm{syn}}$:

$$\hat{S}_{\mathrm{syn}} := \sum_{k_1, k_2, \ldots, k_{n_s} = 0, 1, \ldots, d-1} \hat{S}_1^{k_1} \hat{S}_2^{k_2} \ldots \hat{S}_{n_a}^{k_{n_s}}$$
$$\otimes \mid k_1 k_2 \ldots k_{n_s} \rangle \langle k_1 k_2 \ldots k_{n_s} \mid, \tag{A2}$$

where n_r is the number of redundant qudits and n_a is the number of ancilla qudits. Note that, as shown in Eq. (A2), $n_a = n_s$. By using the circuit shown in Fig. 9, we can store the measurement values of $\{\hat{S}_i\}_{i=1}^{n_s}$ in the ancilla qudits [59].

A.2 Three-qudit repetition code and stabilizer group

Consider a three-qudit repetition code and partial QEC for bit-flipping errors. The initial state of the three-qudit repetition code is given by

$$\mid \tilde{\psi} \rangle := \widehat{\mathrm{CNOT}}_{1,2} \widehat{\mathrm{CNOT}}_{1,3} \mid \psi \rangle \mid 0 \rangle \mid 0 \rangle, \tag{A3}$$

We consider the following stabilizer group for correct bit-flipping errors:

$$\mathcal{S} := \{\hat{Z}_1 \hat{Z}_2^\dagger, \hat{Z}_2 \hat{Z}_3^\dagger\}. \tag{A4}$$

Equation (A4) stabilizes the following states:

$$\{\mid k, k, k \rangle\}_{k=0, 1, \ldots, d-1}. \tag{A5}$$

Note that Eq. (A4) can correct the bit-flipping errors though it cannot correct all one-qudit errors.

A.2.1 Full circuit

In the main text, we clarified that qudits are robust against bit-flipping errors. Our goal is to correct phase-flipping errors via QEC; the circuit shown in Fig. 9 with Eq. (A4) can correct them by inserting quantum Fourier transform (QFT) operators before and after the error models. The full circuit based on the circuit shown in Fig. 9 with Eq. (A4) is given by Fig. 10 where we have used subcircuits shown in Fig. 11, and the
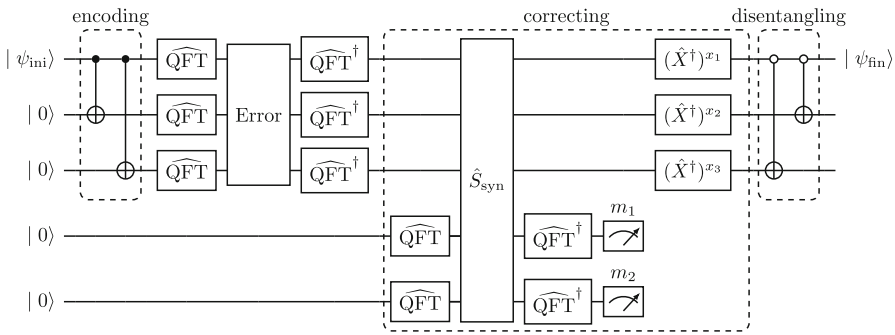
Fig. 10 QEC circuit for phase-flipping errors

Fig. 11 Subcircuits for QEC circuit shown in Fig. 10

$$\vcenter{\hbox{}} := \widehat{\mathrm{CNOT}}_{1,2},$$

$$\vcenter{\hbox{}} := \widehat{\mathrm{CNOT}}_{1,2}^{\dagger}$$
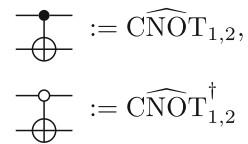
Table 2 Relationship between measurements and correction operators. Only correctable patterns of measurements are shown. In the table, i takes $0, 1, 2, \ldots, d-1$

m_1	m_2	x_1	x_2	x_3
i	0	i	0	0
$-i \ (\mathrm{mod}\ d)$	i	0	i	0
0	$-i \ (\mathrm{mod}\ d)$	0	0	i

measurements are taken in the computational basis by using $\hat{P}^k$ for $k = 0, 1, \ldots, d-1$. Note that $\widehat{\mathrm{CNOT}}_{i,j} \neq \widehat{\mathrm{CNOT}}_{i,j}^{\dagger}$ unlike the conventional CNOT gate.

The correct operators in Fig. 10 are specified by (x_1, x_2, x_3), and they are functions of the values of measurements (m_1, m_2). In Table 2, we summarize the relationship between (m_1, m_2) and (x_1, x_2, x_3).

A.2.2 Numerical results

Figure 12 shows the process fidelity with and without QEC in the case of the Z-type error model by solid and dashed lines, respectively.

Since the QEC circuit in Fig. 10 is designed for phase-flipping errors, the process fidelity with QEC is higher than that without QEC for small p.

Figure 13 shows the process fidelity with and without QEC in the case of the X'-type error model by solid and dashed lines, respectively.

Since the QEC circuit in Fig. 10 cannot correct bit-flipping errors, the process fidelity without QEC is higher than that with QEC.

Figure 14 shows the process fidelity with and without QEC in the case of the $X' + Z$-type error model by solid and dashed lines, respectively.

Figure 14 shows that, though the QEC circuit in Fig. 10 can correct phase-flip errors, the process fidelity without QEC is higher than that with QEC.
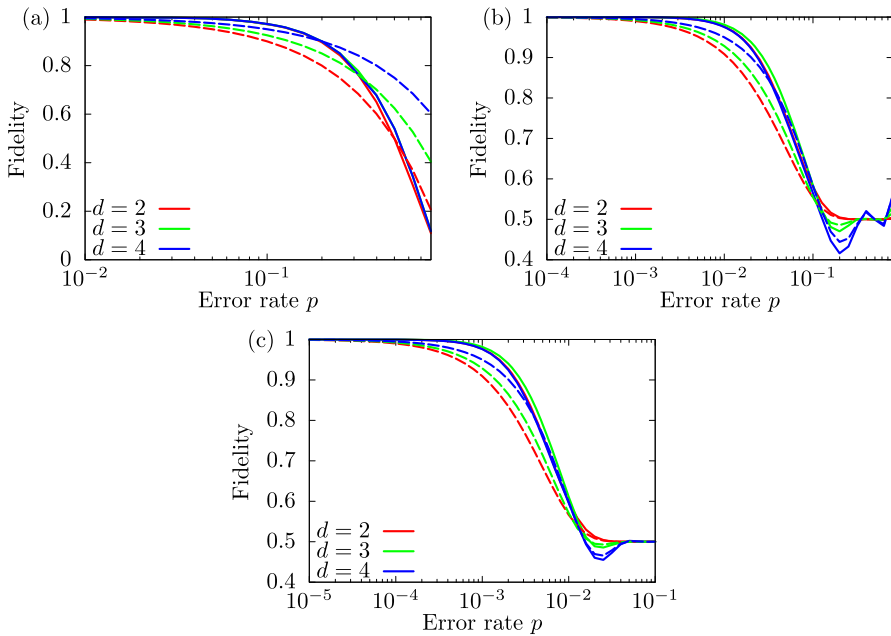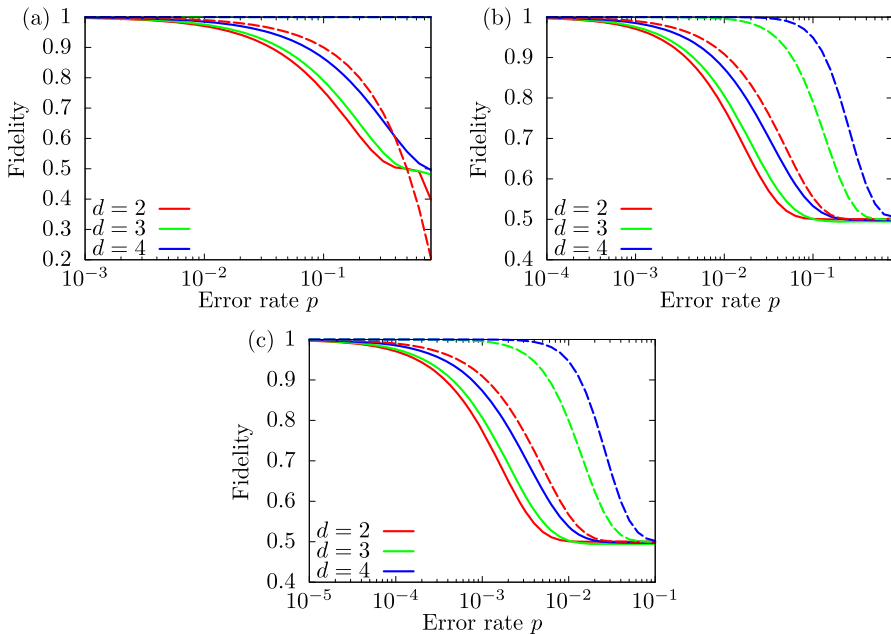
Fig. 12 Process fidelity for the Z-type error model. Solid lines and dashed lines depict results with and without QEC, respectively. We use states at **a** $\tau = 1$, **b** $\tau = 10$, and **c** $\tau = 100$. The initial state is the maximally entangled state

A.3 Remarks

Though QEC for both bit-flipping and phase-flipping errors was not investigated in this paper, it is expected that it can improve the process fidelity. However, to implement QEC for both bit-flipping and phase-flipping errors such as the surface code, a large number of qubits are required. We should note that the QEC we considered for phase-flipping errors is simple. Our simulation results show that the process fidelity is improved only for the Z-type error model but performance gets worse for X'- and $X' + Z$-type error models. This result suggests that the inherent physical robustness of qudits may be an interesting avenue to pursue in conjunction with or in lieu of error-correcting codes, which have higher overhead costs. In order to determine the actual performance gains, a real physical system and its precise characteristics should be modeled.

A.4 Physical justification of the error operators

The operators X' and Z map to known physical systems. Two such physical models are the Cooper-pair box (CPB) model and the Jayne–Cummings model. The Hamiltonian
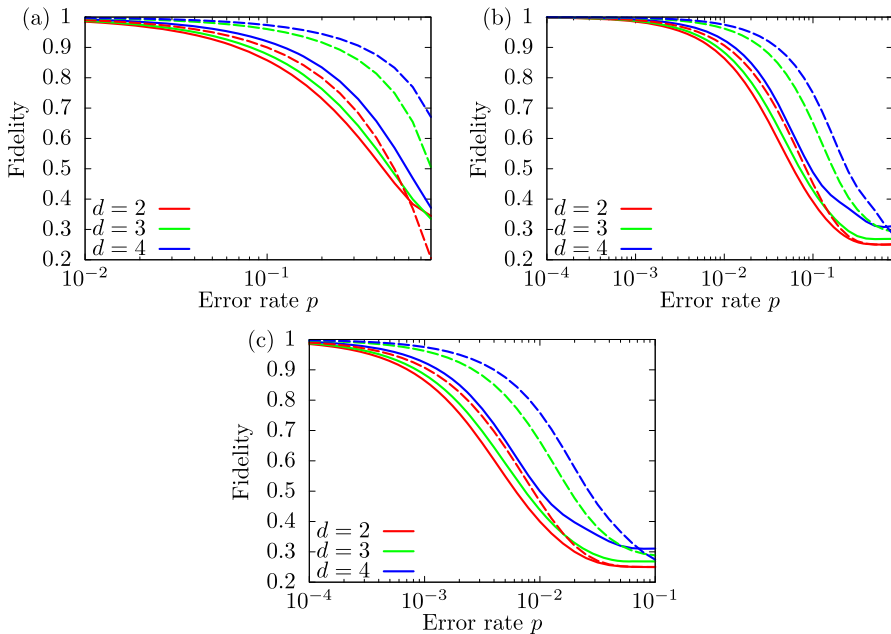
Fig. 13 Process fidelity for the X'-type error model. Solid lines and dashed lines depict results with and without QEC, respectively. We use states at **a** $\tau = 1$, **b** $\tau = 10$, and **c** $\tau = 100$. The initial state is the maximally entangled state

of the CPB model is of the form [75]:

$$
\hat{H}_{\text{CPB}} := \hbar \omega_r \hat{a}^\dagger \hat{a} - \frac{E_J}{2} \sum_N (|\, N \rangle\langle N + 1 \,| + |\, N + 1 \rangle\langle N \,|)
$$
$$
+ 4 E_C \sum_N (N - \hat{n}_g)^2 \,|\, N \rangle\langle N \,|, \tag{A6}
$$

where $\omega_r = \sqrt{LC}$ is the frequency, $\hat{a}$ is the annihilation operator for the microwave resonator field, $\hat{n}_g := \frac{C_g \hat{V}_g}{2e}$, C_g is the capacitance between the CPB island and the bias gate for the island, $E_J/\hbar$ is the Josephson frequency, $E_C := \frac{e^2}{2C_\Sigma}$, and C_Σ is the capacitance between the island and the rest of the circuit. $\hat{V}_g$ is the operator for the total voltage applied to the island by the bias gate. This voltage can be split as $\hat{V}_g = V_g^{(0)} + \hat{v}$, where $V_g^{(0)}$ is a DC field and $\hat{v}$ is the microwave field in the cavity, which is quantized. It is related to the cavity annihilation operator by $\hat{v} = (\hat{a} + \hat{a}^\dagger)\sqrt{\hbar\omega_r/(2C)}$. We can write $\hat{n}_g = n_g^{(0)} + \delta\hat{n}_g$ and $\delta\hat{n}_g(t) = [C_g/(2e)]\hat{v}(t)$. For $\hat{n}_g(t)$ small, the bias $n_g^{(0)}$ can be chosen such that the CPB has a small number of CP on it at any time. Thus, the Hilbert space can be restricted to a smaller subspace, e.g., $N \in \{0, 1, \ldots, d-1\}$. The Cooper-pair operators in the second and third terms then directly map to our operators X' and Z, respectively. Both terms can give rise to decoherence channels for the CPB

Fig. 14 Process fidelity for the $X' + Z$-type error model. Solid lines and dashed lines depict results with and without QEC, respectively. We use states at **a** $\tau = 1$, **b** $\tau = 10$, and **c** $\tau = 100$. The initial state is the maximally entangled state

if terms in their coefficients (E_J, E_C, C_g, C_Σ) fluctuate. For example, fluctuations in the Josephson frequency E_J (second term) can lead to decoherence in a "random-field" semiclassical picture (e.g., Redfield master equation). The decoherence rate is determined by the time autocorrelation $\langle E_J(t)E_J(t+\tau)\rangle$. Since the third term depends on the bath operators a, $a^\dagger$ (via $\hat{v}$), and E_C, decoherence in the quantum master equation at a rate is determined by the time autocorrelation of bath operators, $\langle \hat{u}(t)\hat{u}(t+\tau)\rangle$, where $\hat{u}(t) := E_C(t)C_g(t)\hat{v}(t)$. Thus, X' and Z operators can be used to model decoherence (amplitude and phase damping channels, respectively) in superconducting qubits, where the common sources of noise include fluctuations in the Josephson energy of the junctions, gate charge fluctuations, magnetic field fluctuations, and interactions with photons and phonons [76, 77].

Another Hamiltonian of interest is Jaynes–Cummings, which can be used to model relaxation in NMR [78–80]:

$$\hat{H}_{JC} := \hbar \hat{a}^\dagger \hat{a} + \frac{\hbar \omega_\alpha}{2}\hat{\sigma}^z + \frac{\hbar \Omega}{2}(\hat{a}\hat{\sigma}^+ + \hat{a}^\dagger \hat{\sigma}^-). \tag{A7}$$

where $\vec{\sigma}$ are Pauli matrices for the nuclear spin $I = 1/2$. For larger spins $I > 1/2$, Eq. (A7) can be directly generalized to the qudit case by replacing $\hat{\sigma}^z$, $\hat{\sigma}^+$, and $\hat{\sigma}^-$ by $\hat{J}^z$, $\hat{J}^+$, and $\hat{J}^-$, respectively. For a general spin I, there are $d = 2I + 1$ sublevels and the Wigner matrices are $(2I + 1) \times (2I + 1)$ dimensional. The angular momentum operators $\vec{\hat{J}}$, (where $\vec{\hat{J}} \equiv \vec{\hat{I}}$ for nuclear spins) transforms like rank-1 tensors

(vectors). The matrices X' and Z are similar to those of $\hat{J}_x = (\hat{J}^+ + \hat{J}^-)/2$ and $\hat{J}_z$, respectively. In the Redfield (semiclassical) description, temporal random fluctuations in the local frequency ω_α lead to decoherence (dephasing) at a rate determined by the autocorrelation function $\langle \omega_\alpha(t)\omega_\alpha(t + \tau) \rangle$. Likewise, fluctuations in the drive field Ω (associated with the photon count in the RF/microwave cavity) lead to an amplitude depolarizing channel.

References

1. Feynman, R.P., et al.: Simulating physics with computers. Int. J. Theor. Phys **21**(6/7) (1982)
2. Deutsch, D., Penrose, R.: Quantum theory, the church-turing principle and the universal quantum computer. Proc. R. Soc. Lond. A Math. Phys. Sci. **400**(1818), 97–117 (1985)
3. Deutsch, D., Jozsa, R.: Rapid solution of problems by quantum computation. Proc. R. Soc. Lond. A Math. Phys. Sci. **439**(1907), 553–558 (1992)
4. Lloyd, S.: Universal quantum simulators. Science **273**(5278), 1073–1078 (1996)
5. Shor, P.W.: Algorithms for quantum computation: discrete logarithms and factoring. In: Proceedings 35th Annual Symposium on Foundations of Computer Science, pp. 124–134 (1994)
6. Fowler, A.G., Devitt, S.J., Hollenberg, L.C.: Implementation of shor's algorithm on a linear nearest neighbour qubit array. arXiv:quant-ph/0402196 (2004)
7. Grover, L.K.: A fast quantum mechanical algorithm for database search. In: Proceedings of the Twenty-eighth Annual ACM Symposium on Theory of Computing, pp. 212–219 (1996)
8. Shor, P.W.: Scheme for reducing decoherence in quantum computer memory. Phys. Rev. A **52**, 2493–2496 (1995)
9. Nielsen, M.A., Chuang, I.L.: Quantum Computation and Quantum Information: 10th Anniversary Edition. Cambridge University Press, (2010). https://doi.org/10.1017/CBO9780511976667
10. Bravyi, S.B., Kitaev, A.Y.: Quantum codes on a lattice with boundary. arXiv:quant-ph/9811052 (1998)
11. Kitaev, A.Y.: Fault-tolerant quantum computation by anyons. Ann. Phys. **303**(1), 2–30 (2003)
12. Kitaev, A.: Anyons in an exactly solved model and beyond. Ann. Phys. **321**(1), 2–111 (2006)
13. Bravyi, S., Englbrecht, M., König, R., Peard, N.: Correcting coherent errors with surface codes. NPJ Quant. Inf. **4**(1), 1–6 (2018)
14. Steane, A.M.: A tutorial on quantum error correction. Quant. Comput. Algorith. Chaos, pp 1–32 (2006)
15. Devitt, S.J., Munro, W.J., Nemoto, K.: Quantum error correction for beginners. Rep. Prog. Phys. **76**(7), 076001 (2013)
16. Fowler, A.G., Mariantoni, M., Martinis, J.M., Cleland, A.N.: Surface codes: towards practical large-scale quantum computation. Phys. Rev. A **86**(3), 032324 (2012)
17. Johnson, M.W., Amin, M.H., Gildert, S., Lanting, T., Hamze, F., Dickson, N., Harris, R., Berkley, A.J., Johansson, J., Bunyk, P., et al.: Quantum annealing with manufactured spins. Nature **473**(7346), 194–198 (2011)
18. Arute, F., Arya, K., Babbush, R., Bacon, D., Bardin, J.C., Barends, R., Biswas, R., Boixo, S., Brandao, F.G., Buell, D.A., et al.: Quantum supremacy using a programmable superconducting processor. Nature **574**(7779), 505–510 (2019)
19. Krinner, S., Lacroix, N., Remm, A., Di Paolo, A., Genois, E., Leroux, C., Hellings, C., Lazar, S., Swiadek, F., Herrmann, J., et al.: Realizing repeated quantum error correction in a distance-three surface code. arXiv preprint arXiv:2112.03708 (2021)
20. Zhao, Y., Ye, Y., Huang, H.-L., Zhang, Y., Wu, D., Guan, H., Zhu, Q., Wei, Z., He, T., Cao, S., et al.: Realizing an error-correcting surface code with superconducting qubits. arXiv preprint arXiv:2112.13505 (2021)
21. Leuenberger, M.N., Loss, D.: Quantum computing in molecular magnets. Nature **410**(6830), 789–793 (2001)
22. Castelvecchi, D.: Quantum computers ready to leap out of the lab in 2017. Nature **541**(7635) (2017)
23. Preskill, J.: Quantum computing in the NISQ era and beyond. Quantum **2**, 79 (2018)
24. Cerezo, M., Arrasmith, A., Babbush, R., Benjamin, S.C., Endo, S., Fujii, K., McClean, J.R., Mitarai, K., Yuan, X., Cincio, L., et al.: Variational quantum algorithms. Nat. Rev. Phys. **3**(9), 625–644 (2021)

25. Mitarai, K., Negoro, M., Kitagawa, M., Fujii, K.: Quantum circuit learning. Phys. Rev. A **98**, 032309 (2018)
26. Schuld, M., Bocharov, A., Svore, K.M., Wiebe, N.: Circuit-centric quantum classifiers. Phys. Rev. A **101**, 032308 (2020)
27. Miyahara, H., Roychowdhury, V.: Ansatz-independent variational quantum classifier. arXiv preprint arXiv:2102.01759 (2021)
28. Han, K.-H., Kim, J.-H.: Quantum-inspired evolutionary algorithm for a class of combinatorial optimization. IEEE Trans. Evol. Comput. **6**(6), 580–593 (2002)
29. Arrazola, J.M., Delgado, A., Bardhan, B.R., Lloyd, S.: Quantum-inspired algorithms in practice. arXiv preprint arXiv:1905.10415 (2019)
30. Miyahara, H., Tsumura, K., Sughiyama, Y.: Deterministic quantum annealing expectation-maximization algorithm. J. Stat. Mech: Theory Exp. **2017**(11), 113404 (2017). https://doi.org/10.1088/1742-5468/aa967e
31. Miyahara, H., Sughiyama, Y.: Quantum extension of variational bayes inference. Phys. Rev. A **98**, 022330 (2018)
32. Szkopek, T., Roychowdhury, V.P., Antoniadis, D.A., Damoulakis, J.N.: Physical fault tolerance of nanoelectronics. Phys. Rev. Lett. **106**, 176801 (2011)
33. Chiesa, A., Petiziol, F., Macaluso, E., Wimberger, S., Santini, P., Carretta, S.: Embedded quantum-error correction and controlled-phase gate for molecular spin qubits. AIP Adv. **11**(2), 025134 (2021)
34. Chiesa, A., Macaluso, E., Petiziol, F., Wimberger, S., Santini, P., Carretta, S.: Molecular nanomagnets as qubits with embedded quantum-error correction. J. Phys. Chem. Lett. **11**(20), 8610–8615 (2020)
35. Puri, S., St-Jean, L., Gross, J.A., Grimm, A., Frattini, N.E., Iyer, P.S., Krishna, A., Touzard, S., Jiang, L., Blais, A., Flammia, S.T., Girvin, S.M.: Bias-preserving gates with stabilized cat qubits. Sci. Adv. **6**(34), 5901 (2020)
36. Grimm, A., Frattini, N.E., Puri, S., Mundhada, S.O., Touzard, S., Mirrahimi, M., Girvin, S.M., Shankar, S., Devoret, M.H.: Stabilization and operation of a kerr-cat qubit. Nature **584**(7820), 205–209 (2020)
37. Tacchino, F., Chiesa, A., Sessoli, R., Tavernelli, I., Carretta, S.: A proposal for using molecular spin qudits as quantum simulators of light-matter interactions. J. Mater. Chem. C **9**, 10266–10275 (2021)
38. Chalopin, T., Bouazza, C., Evrard, A., Makhalov, V., Dreon, D., Dalibard, J., Sidorenkov, L.A., Nascimbene, S.: Quantum-enhanced sensing using non-classical spin states of a highly magnetic atom. Nat. Commun. **9**(1), 1–8 (2018)
39. Michael, M.H., Silveri, M., Brierley, R.T., Albert, V.V., Salmilehto, J., Jiang, L., Girvin, S.M.: New class of quantum error-correcting codes for a bosonic mode. Phys. Rev. X **6**, 031006 (2016)
40. Leghtas, Z., Kirchmair, G., Vlastakis, B., Schoelkopf, R.J., Devoret, M.H., Mirrahimi, M.: Hardware-efficient autonomous quantum memory protection. Phys. Rev. Lett. **111**, 120501 (2013)
41. Bergmann, M., van Loock, P.: Quantum error correction against photon loss using multicomponent cat states. Phys. Rev. A **94**, 042332 (2016)
42. Mirrahimi, M.: Cat-qubits for quantum computation. Comptes Rendus Physique **17**(7), 778–787 (2016)
43. Li, L., Zou, C.-L., Albert, V.V., Muralidharan, S., Girvin, S.M., Jiang, L.: Cat codes with optimal decoherence suppression for a lossy bosonic channel. Phys. Rev. Lett. **119**, 030502 (2017)
44. Hastrup, J., Andersen, U.L.: All-optical cat-code quantum error correction. arXiv preprint arXiv:2108.12225 (2021)
45. Gottesman, D., Kitaev, A., Preskill, J.: Encoding a qubit in an oscillator. Phys. Rev. A **64**, 012310 (2001)
46. Tzitrin, I., Bourassa, J.E., Menicucci, N.C., Sabapathy, K.K.: Progress towards practical qubit computation using approximate Gottesman-Kitaev-Preskill codes. Phys. Rev. A **101**, 032315 (2020)
47. Bourassa, J.E., Alexander, R.N., Vasmer, M., Patil, A., Tzitrin, I., Matsuura, T., Su, D., Baragiola, B.Q., Guha, S., Dauphinais, G., et al.: Blueprint for a scalable photonic fault-tolerant quantum computer. Quantum **5**, 392 (2021)
48. Larsen, M.V., Chamberland, C., Noh, K., Neergaard-Nielsen, J.S., Andersen, U.L.: Fault-tolerant continuous-variable measurement-based quantum computation architecture. PRX Quantum **2**, 030325 (2021)
49. Grimsmo, A.L., Combes, J., Baragiola, B.Q.: Quantum computing with rotation-symmetric bosonic codes. Phys. Rev. X **10**, 011058 (2020)
50. Sanctuary, B.C.: Multipole n.m.r. Mole. Phys. **48**(6), 1155–1176 (1983)
51. Zur, Y., Vega, S.: Two-photon nmr on spins with i=1 in solids. J. Chem. Phys. **79**(2), 548–558 (1983)

52. Vega, S., Pines, A.: Operator formalism for double quantum nmr. J. Chem. Phys. **66**(12), 5624–5644 (1977)
53. Vega, S., Naor, Y.: Triple quantum nmr on spin systems with i = 3/2 in solids. J. Chem. Phys. **75**(1), 75–86 (1981)
54. Hostens, E., Dehaene, J., De Moor, B.: Stabilizer states and clifford operations for systems of arbitrary dimensions and modular arithmetic. Phys. Rev. A **71**, 042315 (2005)
55. Pirandola, S., Mancini, S., Braunstein, S.L., Vitali, D.: Minimal qudit code for a qubit in the phase-damping channel. Phys. Rev. A **77**, 032309 (2008). https://doi.org/10.1103/PhysRevA.77.032309
56. Cafaro, C., Maiolini, F., Mancini, S.: Quantum stabilizer codes embedding qubits into qudits. Phys. Rev. A **86**, 022308 (2012). https://doi.org/10.1103/PhysRevA.86.022308
57. Bullock, S.S., Brennen, G.K.: Qudit surface codes and gauge theory with finite cyclic groups. J. Phys. A: Math. Theor. **40**(13), 3481–3505 (2007)
58. Watson, F.H.E., Anwar, H., Browne, D.E.: Fast fault-tolerant decoder for qubit and qudit surface codes. Phys. Rev. A **92**, 032309 (2015)
59. Nadkarni, P.J., Garani, S.S.: Quantum error correction architecture for qudit stabilizer codes. Phys. Rev. A **103**, 042420 (2021)
60. Klappenecker, A., Sarvepalli, P.K.: On subsystem codes beating the quantum hamming or singleton bound. Proc. R. Soc. A Math. Phys. Eng. Sci. **463**(2087), 2887–2905 (2007)
61. Wang, Y., Hu, Z., Sanders, B.C., Kais, S.: Qudits and high-dimensional quantum computing. Front. Phys. **8**, 479 (2020)
62. Gheorghiu, V.: Standard form of qudit stabilizer groups. Phys. Lett. A **378**(5), 505–509 (2014)
63. Breuer, H.-P., Petruccione, F., *et al.*: The Theory of Open Quantum Systems. Oxford University Press on Demand (2002)
64. Liang, Y.-C., Yeh, Y.-H., Mendonça, P.E., Teh, R.Y., Reid, M.D., Drummond, P.D.: Quantum fidelity measures for mixed states. Rep. Prog. Phys. **82**(7), 076001 (2019)
65. Gilchrist, A., Langford, N.K., Nielsen, M.A.: Distance measures to compare real and ideal quantum processes. Phys. Rev. A **71**, 062310 (2005)
66. Mayer, K., Knill, E.: Quantum process fidelity bounds from sets of input states. Phys. Rev. A **98**, 052326 (2018)
67. Kohlrausch, R.: Theorie des elektrischen rückstandes in der leidener flasche. Ann. Phys. **167**(2), 179–214 (1854)
68. Elton, D.C.: Stretched exponential relaxation. arXiv preprint arXiv:1808.00881 (2018)
69. June, R.K., Cunningham, J.P., Fyhrie, D.P.: A novel method for curvefitting the stretched exponential function to experimental data. Biomed. Eng. Res. **2**(4), 153 (2013)
70. Wasilewski, W., Banaszek, K.: Protecting an optical qubit against photon loss. Phys. Rev. A **75**, 042316 (2007)
71. Mehta, K.K., Bruzewicz, C.D., McConnell, R., Ram, R.J., Sage, J.M., Chiaverini, J.: Integrated optical addressing of an ion qubit. Nat. Nanotechnol. **11**(12), 1066–1070 (2016)
72. Hudson, E. private communication
73. Warren, W.S.: Selectivity in multiple quantum nuclear magnetic resonance (1980). https://doi.org/10.2172/7091703
74. Warren, W.S. private communication
75. Schuster, D.I., Wallraff, A., Blais, A., Frunzio, L., Huang, R.-S., Majer, J., Girvin, S.M., Schoelkopf, R.J.: ac stark shift and dephasing of a superconducting qubit strongly coupled to a cavity field. Phys. Rev. Lett. **94**, 123602 (2005). https://doi.org/10.1103/PhysRevLett.94.123602
76. O'Malley, P.J.J.: Superconducting Qubits: Dephasing and Quantum Chemistry. University of California, Santa Barbara (2016)
77. Ithier, G., Collin, E., Joyez, P., Meeson, P.J., Vion, D., Esteve, D., Chiarello, F., Shnirman, A., Makhlin, Y., Schriefl, J., Schön, G.: Decoherence in a superconducting quantum bit circuit. Phys. Rev. B **72**, 134519 (2005). https://doi.org/10.1103/PhysRevB.72.134519
78. Paula, F.M., Silva, I.A., Montealegre, J.D., Souza, A.M., deAzevedo, E.R., Sarthour, R.S., Saguia, A., Oliveira, I.S., Soares-Pinto, D.O., Adesso, G., Sarandy, M.S.: Observation of environment-induced double sudden transitions in geometric quantum correlations. Phys. Rev. Lett. **111**, 250401 (2013). https://doi.org/10.1103/PhysRevLett.111.250401
79. Auccaise, R., Céleri, L.C., Soares-Pinto, D.O., deAzevedo, E.R., Maziero, J., Souza, A.M., Bonagamba, T.J., Sarthour, R.S., Oliveira, I.S., Serra, R.M.: Environment-induced sudden transition in quantum

discord dynamics. Phys. Rev. Lett. **107**, 140403 (2011). https://doi.org/10.1103/PhysRevLett.107.140403

80. Silva, I.A., Souza, A.M., Bromley, T.R., Cianciaruso, M., Marx, R., Sarthour, R.S., Oliveira, I.S., Lo Franco, R., Glaser, S.J., deAzevedo, E.R., Soares-Pinto, D.O., Adesso, G.: Observation of time-invariant coherence in a nuclear magnetic resonance quantum simulator. Phys. Rev. Lett. **117**, 160402 (2016). https://doi.org/10.1103/PhysRevLett.117.160402

Publisher's Note Springer Nature remains neutral with regard to jurisdictional claims in published maps and institutional affiliations.